

Learning UAV-based path planning for efficient localization of objects using prior knowledge

Rick van Essen^{a,*}, Eldert van Henten^a, Gert Kootstra^a

^a*Agricultural Biosystems Engineering, Department of Plant Sciences, Wageningen University and Research, 6700 AA, Wageningen, The Netherlands*

Abstract

UAV's are becoming popular for various object search applications in agriculture, however they usually use time-consuming row-by-row flight paths. This paper presents a deep-reinforcement-learning method for path planning to efficiently localize objects of interest using UAVs with a minimal flight-path length. The method uses some global prior knowledge with uncertain object locations and limited resolution in combination with a local object map created using the output of an object detection network. The search policy could be learned using deep Q-learning. We trained the agent in simulation, allowing thorough evaluation of the object distribution, typical errors in the perception system and prior knowledge, and different stopping criteria. When objects were non-uniformly distributed over the field, the agent found the objects quicker than a row-by-row flight path, showing that it learns to exploit the distribution of objects. Detection errors and quality of prior knowledge had only minor effect on the performance, indicating that the learned search policy was robust to errors in the perception system and did not need detailed prior knowledge. Without prior knowledge, the learned policy was still comparable in performance to a row-by-row flight path. Finally, we demonstrated that it is possible to learn the appropriate moment to end the search task. The applicability of the approach for object search on a real drone was comprehensively discussed and evaluated. Overall, we conclude that the learned search policy increased the efficiency of finding objects using a UAV, and can be applied in real-world conditions when the specified assumptions are met.

Keywords: Deep Reinforcement Learning, Path Planning, Drones

1. Introduction

In recent years, Unmanned Aerial Vehicles (UAVs) are becoming increasingly popular for various applications in agriculture (Rejeb et al., 2022). Examples in agriculture are finding weeds or diseased plants in

*Corresponding author.

Email address: rick.vanessen@wur.nl (Rick van Essen)

large arable fields (Albani et al., 2019; Chin et al., 2023), detecting cattle in pastures (Rivas et al., 2018; Liu et al., 2021) and blossom detection in orchards (Zhang et al., 2023). Generally, these applications have a main task: to find objects of interest in an area larger than the field-of-view (FoV) of the UAV, which requires the UAV to fly over the field. A limitation of using UAVs for these applications is their limited battery capacity (Rejeb et al., 2022; Guban and Haque, 2023). Therefore it is important to find a path between all the objects of interest that minimizes the UAV’s flight time in order to increase the area that can be inspected in a single flight.

When these objects are uniformly distributed over the area, a coverage path planner covering the entire search area is suitable and efficient. However, in applications where the objects are non-uniformly distributed, it may be more efficient to use a search policy that searches for objects instead of covering the whole area. A task such as the detection of weeds is an example of an application with non-uniformly distributed objects, since some weed species occur in distinct patches in a field (Cardina et al., 1997; Xu et al., 2023a). A lot of work is done on weed detection using drone images (Xu et al., 2023b; Anul Haq, 2022; Pei et al., 2022), however they all follow predefined, row-by-row, flight paths.

Over the last years, Reinforcement Learning (RL) has gained more attention in path planning for both mobile robots (Yu et al., 2020; Gao et al., 2020; Niroui et al., 2019) as well as UAVs (Azar et al., 2021; Tu and Juang, 2023). These RL-based methods can learn search strategies through interaction with the environment by maximizing the information gathered in an environment (Lodel et al., 2022). RL offers several advantages for path planning: it does not need a detailed map of obstacles in the environment, can deal with noisy sensor information (Gao et al., 2020) and can learn spatial relations between objects of interest in the environment. When trained, a RL learned policy makes sequential decisions about the direction of the robot or drone with relatively short calculation times, as compared to traditional methods like Dijkstra’s algorithm, A* and D* (Tu and Juang, 2023). This allows for online path planning, eliminating the need to calculate the complete path in advance. Using RL it is possible to plan paths with less or uncertain prior knowledge about the environment (Yu et al., 2020; Guban and Haque, 2023), and thereby making path planning more flexible and reactive to a changing environment.

Several works have studied path planning using RL. Panov et al. (2018) and Yu et al. (2020) showed that a trained RL network is able to generate a policy to move an agent in a grid-based world to a target location while avoiding obstacles. A novel neural network architecture for coverage path-planning and object search was introduced by Theile et al. (2020, 2021), combining detailed high-resolution local information with low resolution global information. However, these approaches assume full prior knowledge about the location of

the target objects and the obstacles, which in many applications is uncertain or even absent. As example, the location of weeds in a field may not be exactly known beforehand, however, some prior knowledge can be derived from the locations of the weeds during the previous year.

When having full prior knowledge, there is enough information to stop the search task when all objects are found. However, when the prior knowledge becomes more sparse and unreliable, the number of objects might be unknown. This makes the end of the search task undefined. Yang et al. (2018) and Druon et al. (2020) used a learned stopping action, where the agent could decide to stop searching when it was not profitable anymore.

Training a RL agent requires huge amounts of data as it needs to explore an enormous state-action space (Gugan and Haque, 2023). To train a RL agent to localize objects in a field, we need the agent to collect a very large amount of training data containing a large variety in object locations in the field and allowing it to explore different policies. Because this is infeasible to achieve in the real world, we trained the agent using simulations, as is commonly done in literature, e.g. Azar et al. (2021); Gao et al. (2020); Theile et al. (2020, 2021); Panov et al. (2018); Yu et al. (2020). We ensured the simulation was realistic, as explained in the next paragraph. An additional benefit of a simulation is that we can investigate the effect of different object distributions, detection inaccuracies and prior knowledge uncertainty in greater detail and with a much higher number of repetitions than would be feasible in real-world experiments and thereby shows the practical potential of such RL based path planner for localizing objects of interest in a field.

In this paper, we propose an RL-based path planner that works on a higher abstraction level, getting a local object map extracted from a perception module based on a camera image, and providing actions in terms of flight directions, that would be executed by a drone’s flight controller. Figure 1 illustrates how the resulting simulation-trained policy can be used in the real-world to control the drone. The drone’s camera image, containing variations in the object appearance due to, e.g., lightning conditions and natural variation, is converted to a local object map using an object detection network. The resulting object coordinates are placed in an object map, which is then used as input to the RL policy. The policy determines the action with respect to the highest expected reward. The discrete output actions (fly north, east, west, south) are then translated to motor commands, by the drone’s flight controller. This abstraction allows us to train the RL agent in simulation.

It is important, however, that the abstract simulation includes typical errors in a perception model and a flight controller. The typical errors in translating the image into object coordinates are false positive and false negative detections and inaccuracies in the location of the detections. These are included in the

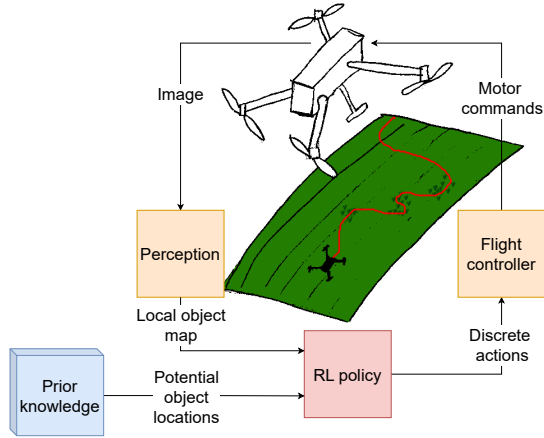


Figure 1: High-level drone control using Reinforcement Learning (RL) in combination with a local object map from a perception system and some potential object locations from the prior knowledge. The output of the detection network is used together with prior knowledge as input for the RL policy, the resulting discrete actions are then translated by the drone’s flight controller to motor commands.

simulation as explained in the materials section. Furthermore, the simulation makes some assumptions about the system: (a) it is assumed the drone is able to accurately execute discrete flight actions, such as fly one meter in a specific direction, (b) a maximum field size based on the number of grid-cells in the simulation and the area of each cell, (c) prior knowledge of the field shape and boundaries, (d) a trained detection network and (e) some potential locations of objects of interest.

The objective of this paper is to develop and evaluate a RL-based method for path planning to efficiently localize objects of interest using UAVs with a minimal path length. Despite being a simulation study, we provide an important contribution to a real-world application by analyzing the effects of the spatial distribution of the objects of interest, typical errors in detection network output and of the typical errors associated with prior knowledge. The real world application is discussed at length in section 4.5. Specifically, we study (1) the effect of the distribution of the objects, (2) the effect of detection errors, (3) the effect of the quality of prior knowledge and finally, and (4) the effect of different stopping criteria.

2. Materials and Methods

In this chapter, we describe the simulation environment, problem statement, the used RL method and the experiments.

2.1. Simulation environment

The field is simulated as a squared grid of $M \times M \in \mathbb{N}^2$ grid cells, where \mathbb{N} is the set of natural numbers. The real-world size of each grid cell depends on the required spatial resolution, which is not part of the simulation environment. In this field, the number of objects, n is drawn from a normal distribution $\mathcal{N}_{\text{obj}}(\mu, \sigma)$. These objects are then distributed according to k different multivariate Gaussian distributions, where k is drawn from $\mathcal{N}_{\text{dist}}(\mu)$. Each Gaussian distribution $\mathcal{N}(\mu_i, \Sigma_i)$ has a random mean μ_i and a random covariance $\Sigma_i \in \{\Sigma_1, \Sigma_2\}$. By randomly distributing the objects in each simulation, we ensure that the RL agent is reactive to the information gathered from the environment, rather than learning the specific locations of each object.

A drone is flying over the field at a fixed altitude and has a camera with a FoV of size $F \times F \in \mathbb{N}^2$ facing downwards. The goal of the drone is to find all objects in the field as fast as possible. The drone can either start at the top-left or bottom-right part of the field, which is randomly selected. For experiment 1 - 3, the simulation terminates when all the objects are found, in experiment 4 we use a learned stop signal. Figure 2 shows two examples of the simulation environment.

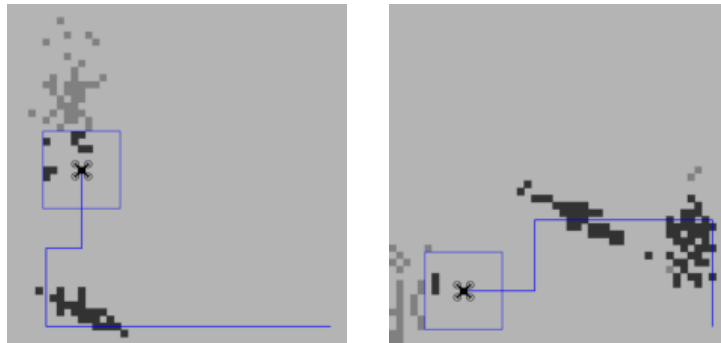


Figure 2: Two examples of the simulation environment with the field-of-view indicated by the blue rectangle around the drone, the flight path in blue, the detected objects in dark-grey and the not-yet-detected objects in light-gray.

The output of the detection network is simulated by creating a map of the objects that are visible within the FoV. Typical errors in the output of a detection network are False Positives (FPs), False Negatives (FNs) and positional errors. FP detections are simulated by adding $r_{\text{dt,fp}} \cdot F^2$ FP detections at a random location in the FoV where $r_{\text{dt,fp}}$ is the fraction FP detections with respect to the size of the FoV, F . FN detections are simulated by removing $r_{\text{dt,fn}} \cdot n_{\text{fov}}$ detections from the visible objects in the current FoV of the drone, where $r_{\text{dt,fn}}$ is the fraction of FN detections with respect to the number of objects visible in the current FoV, n_{fov} . Uncertainty in the position of the objects in the detection map is simulated by adding an offset drawn from the normal distribution $\mathcal{N}_{\text{dt,pos}}(0.0, \sigma)$, independently in both x and y directions. These

errors are simulated independently for each detection.

The prior knowledge is based on a map of ground truth locations of objects in the simulation. Inaccuracies in the prior knowledge are simulated by adding $r_{\text{pk,fp}} \cdot M^2$ false positives, where $r_{\text{pk,fp}}$ is the fraction of FPs in the prior knowledge with respect to the world size M . FNs in the prior knowledge are simulated by removing $r_{\text{pk,fn}} \cdot n$ objects from the ground truth map with the object locations where $r_{\text{pk,fn}}$ is the fraction of FNs with respect to the number of objects n . Same as for the detection network output, the location of the objects is altered by drawing an offset from the normal distribution $\mathcal{N}_{\text{pk,pos}}(0.0, \sigma)$. To simulate a reduction in resolution, the map is down-sampled using average pooling with a kernel size of $\lfloor \frac{M}{P} \rfloor$ where $P \times P$ is the resulting prior knowledge size. The prior knowledge is simulated once for each simulation.

2.2. Problem definition

To solve the described goal, the simulation is implemented as a Markov Decision Process (MDP). A MDP is described by a state-space S , an action-space A and a reward R (Sutton and Barto, 2018). In a state $s_t \in S$ at timestep t , an agent (the drone) performs an action $a_t \in A$ yielding a transition to state $s_{t+1} \in S$ and a reward $r_t \in R$.

The state-space representation, S , is adapted from Theile et al. (2021), containing a global and local map representation and a movement budget scalar. The global map contains down-sampled information about the complete field (the prior knowledge) and the local map contains detailed information about the current FoV of the drone (representing the output of the detection network). Both global and local maps consist of three layers: a field-area layer, a layer with the locations of the already detected objects, and a third layer consisting of the prior knowledge for the global map and simulated detection network output for the local map. The field-area layer describes the area of the field (value of 0) and the area outside the field (value of 1). The layer with the already detected objects contains a value of 1 at the places where objects have been detected and 0 at all other locations. The movement budget scalar b equals the remaining battery capacity and is calculated by $b = b_{\text{init}} - s \cdot b_{\text{step}}$, where b_{init} is the initial battery level of the drone, s the number of flight actions made in the field, and b_{step} the battery usage of each step.

Both the global and the local map are drone-centric, meaning that the drone is always in the middle of the map. Work by Theile et al. (2021) showed that centering the local and global map makes it possible to scale to larger fields. To do so, the global map is padded to a size of $(2M - 1) \times (2M - 1)$ by adding padding values of 0 for both the detected object and prior knowledge layer and values of 1 for the field-area layer (indicating that the drone is not allowed to fly outside the field). To decrease the size of the global map, the global map is down-sampled using average pooling with kernel size g_{global} resulting in a global map size

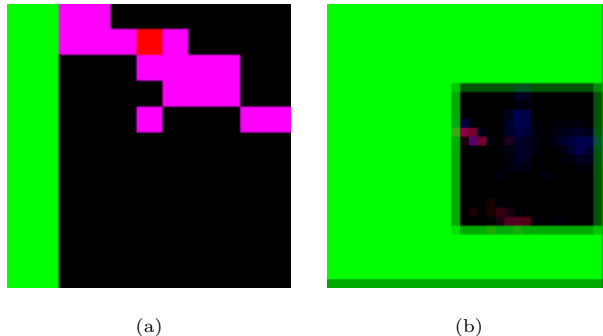


Figure 3: Example of the local (a) and global (b) map. Red indicates the already detected objects, green the area outside the field and blue the simulated output of a detection network for the local map and the prior knowledge for the global map. Note that purple is a combination red and blue.

of $\frac{2M-1}{g_{\text{global}}} \times \frac{2M-1}{g_{\text{global}}}$. The local map is padded to a size of $F \times F$ by adding padding values of 0 for both the detected object map and output of the detection network, and values of 1 for the field-area layer when the FoV partly extends outside the field. An example of the global and local map is shown in Figure 3.

The action-space, A , contains the following actions: fly north, fly south, fly east and fly west. Each fly action moves the drone one grid cell in the associated direction. The drone cannot move into the area outside the field. For experiment 4, we added another 'land' action, that terminates the search.

For each timestep t , the reward function, $r(s_t, a_t)$, yields a positive reward, r_{dt} , for every detected weed, a negative reward, r_{nfz} , for trying to fly into the area outside the field and a small negative reward, r_{step} , for every action. A large negative reward, r_{crash} , is given when the drone runs out of battery before the task is completed, as it would crash.

The default parameters for the simulation are given in Table 1. The simulation is implemented using the OpenAI Gym API and made available on GitHub¹.

2.3. Policy learning

The goal of RL is to find a policy $\pi(s)$ that specifies an action $a \in A$ given state $s \in S$. The control policy of the drone can be described by:

$$\pi(s_t) = \underset{a \in A}{\operatorname{argmax}} Q(s_t, a), \quad (1)$$

where $Q(s, a)$ is the learned action-value function. Q-learning is a popular model-free method that learns the action-value function by iteratively optimizing a Q-table using the immediate reward r_t and the discounted

¹https://github.com/wur-abe/rl_drone_object_search

Table 1: Parameters for the default simulation environment.

Parameter	Value	Description
M	48	Field size
$\mathcal{N}_{\text{obj}}(\mu, \sigma)$	$\mathcal{N}(100, 30)$	Number of objects
$\mathcal{N}_{\text{dist}}(\mu, \sigma)$	$\mathcal{N}(3, 2)$	Number of distributions
Σ_1	$\begin{bmatrix} 5 & 8 \\ 8 & 20 \end{bmatrix}$	Covariance distribution 1
Σ_2	$\begin{bmatrix} 20 & 0 \\ 0 & 0 \end{bmatrix}$	Covariance distribution 2
F	11	FoV size of the drone
$r_{\text{dt,fp}}$	0.05	Detection FP
$r_{\text{dt,fn}}$	0.0001	Detection FN
$\mathcal{N}_{\text{dt,pos}}(0.0, \sigma)$	$\mathcal{N}(0.0, 0.2)$	Detection offset
$r_{\text{pn,fn}}$	0.20	Prior knowledge FP
$r_{\text{pk,fn}}$	0.001	Prior knowledge FN
$\mathcal{N}_{\text{pk,pos}}(0.0, \sigma)$	$\mathcal{N}(0.0, 0.5)$	Prior knowledge offset
P	12	Prior knowledge resolution
g_{global}	3	Global map kernel size
b_{init}	75	Initial battery level
b_{step}	0.2	Battery usage per step
r_{dt}	1.0	Detection reward
r_{nfz}	-1.0	Hit no-fly-zone reward
r_{step}	-0.2	Step reward
r_{crash}	-150.0	Crash reward

future reward $\gamma \cdot \max_{a \in A} Q(s_{t+1}, a)$, where $\gamma \in [0, 1]$ is the discount factor determining the emphasis on the future reward (Sutton and Barto, 2018). Q-Learning is, however, unsuitable for learning high-dimensional state-spaces because the size of the Q-table grows exponentially with the number of possible states and actions. To overcome this problem, we used a Deep Q-Network (DQN) introduced by Mnih et al. (2015). DQN uses a neural network to approximate the action-value function. The architecture of this network is described in section 2.3.1. Section 2.3.2 describes the experience replay buffer which is used to provide training samples for the network. The training procedure is described in section 2.3.3.

2.3.1. Network architecture

Figure 4 shows the used network architecture for the Q-network. The network gets the current state s_t as input and predicts the Q-value for every action $a \in A$. The network consists of a feature extractor and a fully connected network. The feature extractor consist of two parallel convolution blocks to ensure unique feature extraction from both local and global map. The output of both convolution blocks is flattened and concatenated with the movement budget to combine the extracted features of the local and global map with the movement budget. Four fully-connected layers convert these features into four outputs which correspond to the action values for each possible action $a \in A$. This architecture is based on the architecture used in Theile et al. (2021).

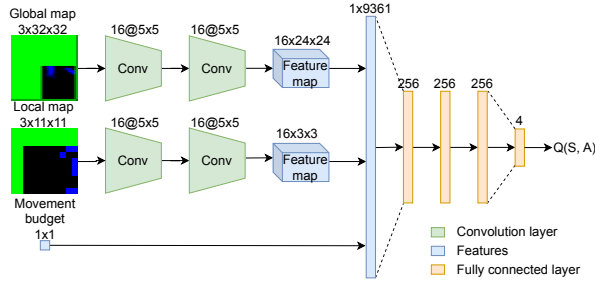


Figure 4: Network architecture for the DQN using the global and local map and the movement budget indicating the input size, the number of kernels and their size, the size of the flatten layer and the size of the fully connected layers. The number of trainable parameters equals 2,544,548.

2.3.2. Experience Replay Buffer

To create training data for the DQN, we used an experience replay buffer (Mnih et al., 2015). The replay buffer is a circular buffer of size n_{buffer} containing state transition vectors, $[s_t, a_t, r_t, s_{t+1}]$. From this buffer, mini-batches of size n_{batch} are sampled for training the Q-network. The buffer is filled by an agent that operates in the simulation following a probability-based training policy that takes random actions from action space A using probability vector p :

$$\forall a \in A, p(s, a) = \frac{\exp(Q(s, a)/\tau)}{\sum_{\forall a_i \in A} \exp(Q(s, a_i)/\tau)}, \quad (2)$$

where $\tau \in (0, \infty)$ is the temperature parameter. A high value for τ gives all actions equal probability and a low value results in a greedy training policy (Equation 1). This probability-based training policy has an advantage over a standard ϵ -greedy policy because τ is independent of the number of training steps, whereas ϵ usually requires a schedule to decrease with the number of training steps. The training policy is implemented in a similar way as Theile et al. (2020).

2.3.3. Training procedure

Figure 5 shows the training procedure for the DQN. During training, two identical neural networks are used: a policy network Q and a target network Q_{target} . The weights of the target network are replaced by the weights of the policy network every n_{update} training steps. This is done to stabilise the learning by reducing the correlation between the action values $Q(s, a)$ and the target value (immediate reward + discounted future rewards) (Mnih et al., 2015). The optimal action-value function is approximated by minimizing the smooth L1 loss (Girshick, 2015) between the target, $y = r_t + \gamma \max_{a_i \in A} (Q_{\text{target}}(s_{t+1}, a_i))$, and the predicted value, $\hat{y} = Q(s_t, a_t)$, using $\beta = 1$. Optimizing the weights of Q is done using an Adam optimizer with

learning rate α .

Optimization of the policy network was started after the replay buffer was filled for 50% and was optimized for n_{steps} training steps. The best weights were selected based on the highest mean reward observed over a validation set of n_{val} evaluation episodes (sequences of steps in a simulation).

Table 2 shows the parameters used during training. The implementation of DQN in Stable-Baselines3 (Raffin et al., 2021) was used with a custom feature extractor and custom training policy. Training was done on a computer with an AMD Ryzen 5950x CPU and NVIDIA RTX 3090 graphics card using 12 parallel simulation environments.

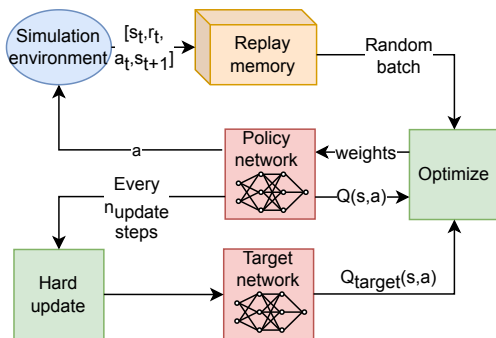


Figure 5: Training procedure for the Deep Q-Network.

Table 2: Hyper-parameters for training the Deep Q-Network.

Parameter	Value	Description
n_{buffer}	50000	Experience replay buffer size
n_{batch}	128	Mini-batch size
τ	0.005	Temperature parameter
γ	0.95	Discount factor
α	$3 \cdot 10^{-5}$	Learning rate
n_{update}	250	Target update rate
n_{steps}	10^7	Training timesteps
n_{val}	120	Number of validation episodes

2.4. Experiments

In this section, we present the experiments to validate the learned search policy. We evaluate the percentage of objects found and flight path length. These values are compared to a traditional row-by-row coverage flight path, planned by Fields2Cover (Mier et al., 2023), using the size of the FoV, F , as path width without overlap. Because we expected the learned path planner to outperform a row-by-row flight path specifically for non-uniformly distribution objects, we evaluated the impact of these object distributions (section 2.4.1). To test the robustness of the RL-learned path planner, we evaluated the effect of detection

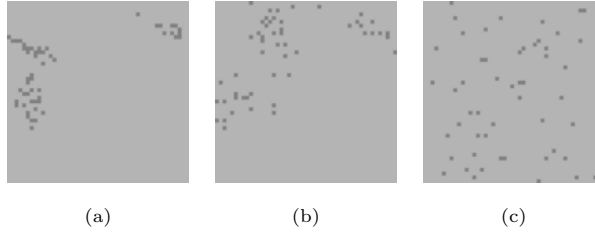


Figure 6: Example of a field with (a) a strong distribution, (b) a medium distribution and (c) a uniform distribution of objects.

errors (section 2.4.2) and prior knowledge quality (section 2.4.3). Lastly, the effect of different stopping criteria was evaluated to mark the end of the search (section 2.4.4).

2.4.1. Experiment 1: Impact of object distributions

To study the influence of the object distribution on the path length and percentage of found objects, three object distributions were defined. Distribution 'strong' was a strong clustered distribution and used the default field parameters from Table 1. Distribution 'medium' was a medium clustered distribution with $\mathcal{N}_{\text{dist}}(\mu, \sigma) = \mathcal{N}(4, 1)$ and $\mathcal{N}(\mu_i, \Sigma_i)$ has a random mean μ_i and a covariance Σ_i uniformly sampled from set $\{\Sigma_1, \Sigma_2, \Sigma_3, \Sigma_4\}$ where $\Sigma_1 = \begin{bmatrix} 10 & 16 \\ 16 & 40 \end{bmatrix}$, $\Sigma_2 = \begin{bmatrix} 40 & 0 \\ 0 & 10 \end{bmatrix}$, $\Sigma_3 = \begin{bmatrix} 30 & 12 \\ 12 & 12 \end{bmatrix}$, and $\Sigma_4 = \begin{bmatrix} 15 & 4 \\ 4 & 20 \end{bmatrix}$. Distribution 'uniform' was a uniform distribution with each object having a uniform random non-overlapping coordinate in the field. For all distributions, the number of objects in the field was drawn from the same normal distribution $\mathcal{N}_{\text{obj}}(\mu, \sigma)$. An example of each distribution is shown in Figure 6. A different policy was trained and evaluated using 1000 evaluation episodes for the three distributions.

2.4.2. Experiment 2: Influence of detection errors

To assess the influence of errors of the simulated detection network on the policy, we defined five detection error levels, ranging from a very high number of errors to no errors. The parameters for each level of detection errors are given in Table 3. The default simulation environment from table 1 is equivalent to the moderate level in table 3. Figure 7 shows an example of the simulated output of the detection network. For each level of detection errors, a policy was trained and evaluated using 1000 evaluation episodes.

Table 3: Error levels for the simulated detection network.

Error level	$r_{\text{dt,fp}}$	$r_{\text{dt,fn}}$	$\mathcal{N}_{\text{dt,pos}}(0, \sigma)$
very high	0.01	0.5	$\mathcal{N}(0, 0.5)$
high	0.001	0.1	$\mathcal{N}(0, 0.1)$
moderate	0.0001	0.05	$\mathcal{N}(0, 0.05)$
low	0.00005	0.02	$\mathcal{N}(0, 0.02)$
perfect	0.0	0.0	$\mathcal{N}(0, 0)$

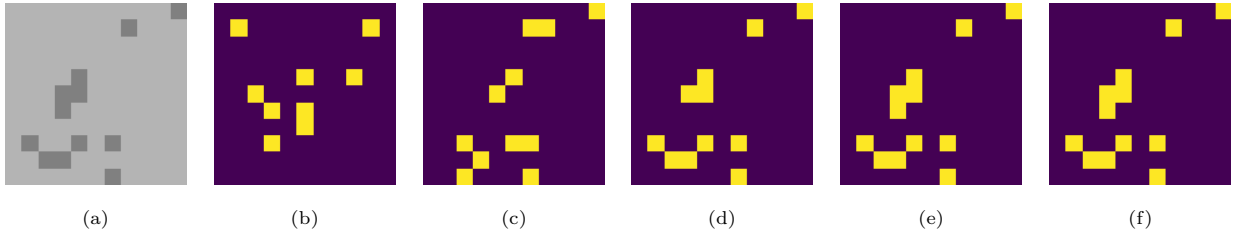


Figure 7: Example of field-of-view (a) and the corresponding simulated detection network output for a very high (b), high (c), moderate (d), and low (e) number of detection errors, and a perfect (f) detector. For visibility, a colormap is applied.

2.4.3. Experiment 3: Influence of prior knowledge quality

We assessed two aspects of quality in the prior knowledge: the uncertainty related to resolution and the inaccuracy in the prior knowledge. When the resolution of the prior knowledge is low, only sparse information about the location of the objects is available. This could, for example, be information from other sources with a lower spatial resolution such as satellite images or images taken from a higher altitude. Another aspect of prior knowledge is the inaccuracy. The higher the inaccuracy, the less reliable the prior knowledge becomes. This could for example be due to sensor noise or detection errors. We defined five levels of prior knowledge quality, ranging from no prior knowledge (level none) to perfect prior knowledge (level perfect), expressing an increasing quality. Table 4 defines these levels. The default simulation environment from table 1 is equivalent to the moderate level in table 4. To keep the same number of trainable parameters in the DQN, we kept the same number of cells in the prior knowledge map for all quality levels by using nearest neighbor upsampling to resize the prior knowledge map to 48×48 . Figure 8 shows an example of the prior knowledge map for each level. For each quality level, a different policy was trained and evaluated using 1000 evaluation episodes.

Table 4: Prior knowledge quality levels.

Quality level	P	$r_{\text{pk,fp}}$	$r_{\text{pk,fn}}$	$\mathcal{N}_{\text{pk,pos}}(0, \sigma)$
none	0x0	-	-	-
low	2x2	0.002	0.40	$\mathcal{N}(0, 1.0)$
moderate	12x12	0.001	0.20	$\mathcal{N}(0, 0.5)$
high	24x24	0.0005	0.05	$\mathcal{N}(0, 0.25)$
perfect	48x48	0.0	0.0	$\mathcal{N}(0, 0)$

2.4.4. Experiment 4: Effect of different stopping criteria

In a real-world application, the number of objects might be unknown which makes the termination of the simulation when all objects are found infeasible. Therefore, we evaluated the effect of different stopping

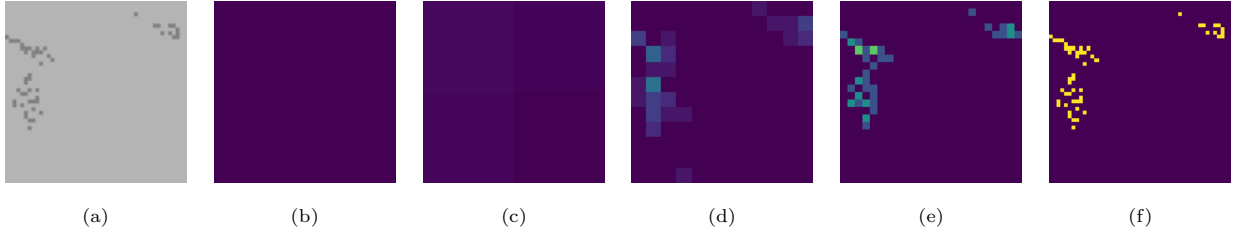


Figure 8: Example of the prior knowledge of world (a) for quality level none (no prior knowledge) (b), low (c), moderate (d), high (e), and perfect (f). Level perfect has high-resolution knowledge about the locations of the objects, while level low has limited knowledge about the locations of objects. For visibility, a colormap is applied.

criteria, specifically:

1. Stop searching when a certain percentage of the field is covered. Two levels were tested, 50% and 75%.
2. Stop searching when there are no new objects detected for a certain number of flight actions. To avoid constantly resetting this counter due to FP detections, at least 2 objects need to be detected. Three thresholds were tested, 15, 25 and 50 steps.
3. A learned landing action, by extending action space A with a 'land' action that terminates the search.

These stopping criteria were compared with the default stopping criterion which stops searching when all objects are found. We compared both the percentage of found objects and the path length. For each stopping criterion, a separate policy was trained and evaluated on 1000 evaluation episodes.

3. Results

3.1. Experiment 1: Impact of object distributions

Figure 9 shows the relation between flight path length and the percentage of found objects for different distributions of objects. The more uniformly distributed the objects were, the more linear the relation between path length and number of found objects. For the strong and medium distributions, the learned policy outperformed the baseline row-by-row flight path, having found more than 80% of the objects in 73 and 94 steps on average respectively, compared to 209 steps for the baseline row-by-row flight path. However the learned policy often had troubles to find all objects before the battery was empty.

Figure 10 shows examples of a single flight path for the strong, medium and uniform distributions, respectively. It can be seen that the drone flew in quite straight lines till around 80% of the objects were found. After 80% the drone started wandering around till the battery was empty and crashed, because the drone missed some objects and environment did only terminate when all objects were found.

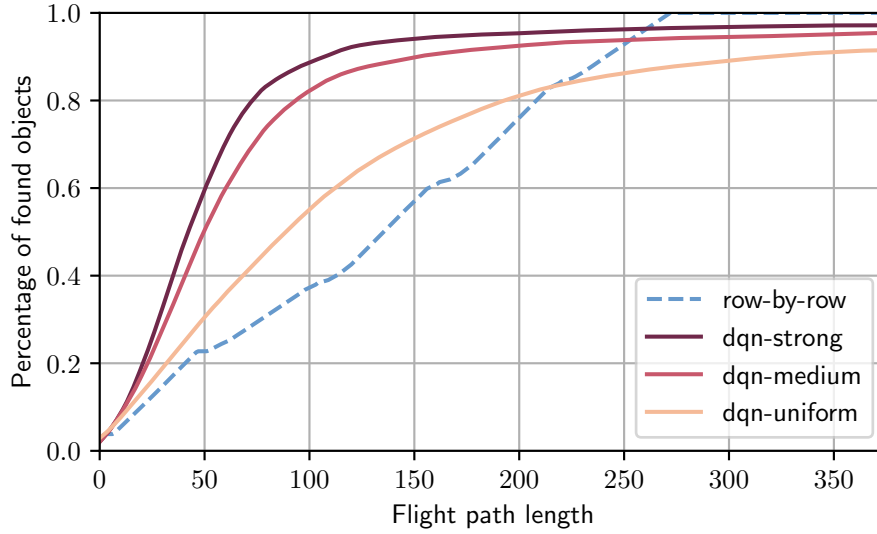


Figure 9: Effect of a strong, a medium and a uniform weed distribution on both the number of found objects and the path length for the policy learned by DQN, and the baseline row-by-row flight path. The lines show the mean over 1000 episodes.

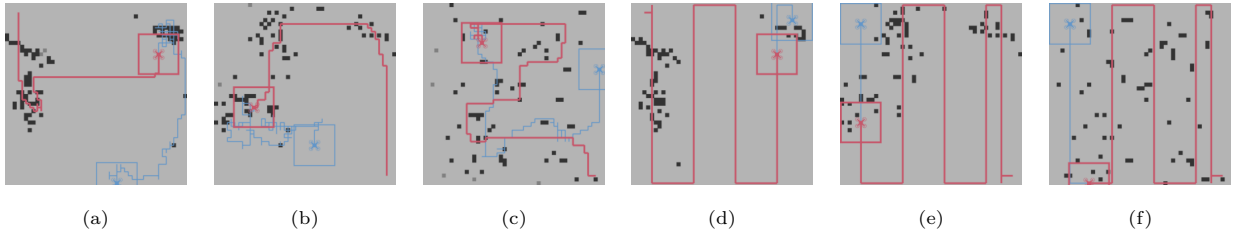


Figure 10: Single flight paths of the RL agent (a-c) and the baseline row-by-row flight path (d-f) for strong (a,d), medium (b,e) and uniform (c,f) distribution of objects. The detected objects are indicated with black dots and the not detected objects with gray dots. The red line indicates the flight path till 80% of the objects are found, the blue line the complete flight path till all objects were found or the battery was empty.

3.2. Experiment 2: Influence of detection errors

Figure 11 shows the relation between the different levels of detection errors and the percentage of found objects and flight path length. All the levels outperformed the baseline row-by-row flight path. The learned policy is robust and only starts to drop performance for a very high number of detection errors. All levels outperform the baseline by having found 80% of the objects in 70 - 98 steps compared to 206 steps for the baseline row-by-row flight path.

Figure 12 shows some flight paths for the different levels of detection errors. For a very high number of detection errors (Figure 12a), there are many false positive detections visible. When having a perfect detection network (Figure 12e), the agent missed some objects, however, this is just an example of a single flight path. On average, this level of detection errors performed comparable to the levels low-high (Figure

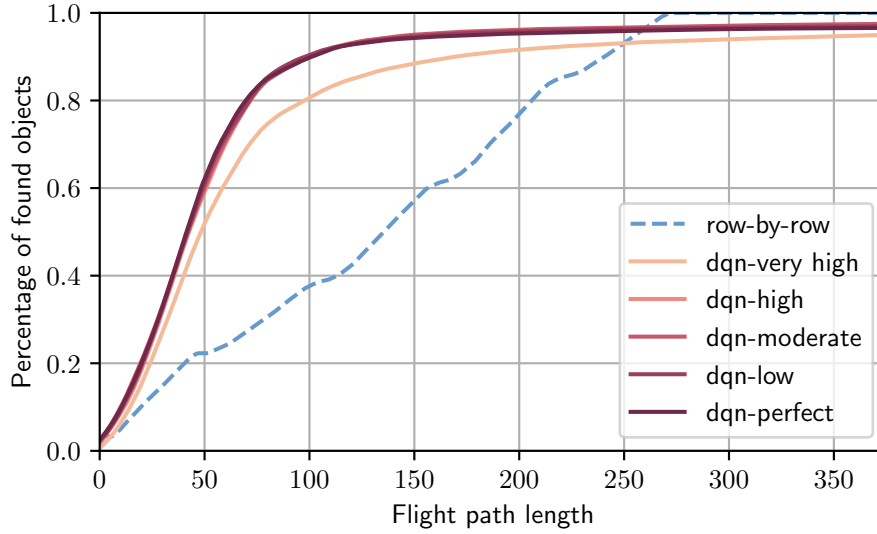


Figure 11: Effect of the different levels of detection errors on the percentage of found objects for the policy learned by DQN, and the baseline row-by-row flight path. The lines show the mean over 1000 episodes.

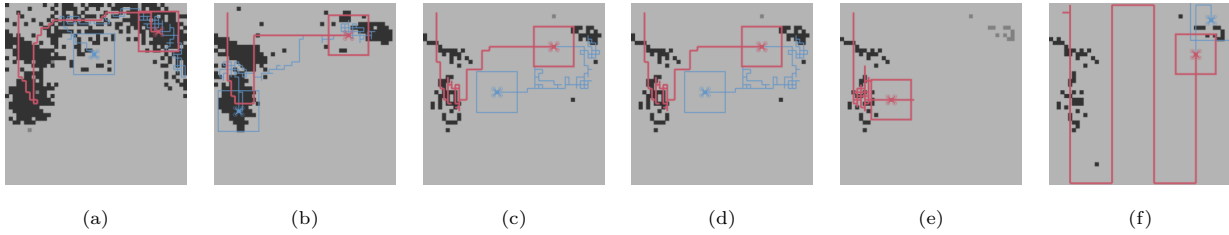


Figure 12: Single flight paths of the RL agent for detection error levels very low (a), low (b), moderate (c), high (d) and perfect (e) and the baseline row-by-row flight path (f). The detected objects are indicated with black dots and the not detected objects with gray dots. The red line indicates the flight path till 80% of the objects are found, the blue line the complete flight path till all objects were found or the battery was empty.

11).

3.3. Experiment 3: Influence of prior knowledge quality

Figure 13 shows the relation between flight path length and the number of found objects for different levels of prior knowledge quality. When having a perfect prior knowledge map without mistakes, the DQN learned a policy that found all objects. Even for prior knowledge of low quality, the DQN learned a policy to quickly find most objects. However, not all objects were found before the battery was empty. The higher the quality of the prior knowledge, the more objects were found. In complete absence of prior knowledge (level none) the agent still found some objects, however, a row-by-row flight path is more efficient in that case. The levels moderate and above outperformed the baseline by having found more than 80% of the objects in 71, 69 and 67 steps respectively compared to 206 steps for the row-by-row flight path. Level low

needed around 300 steps to find 80% of the object.

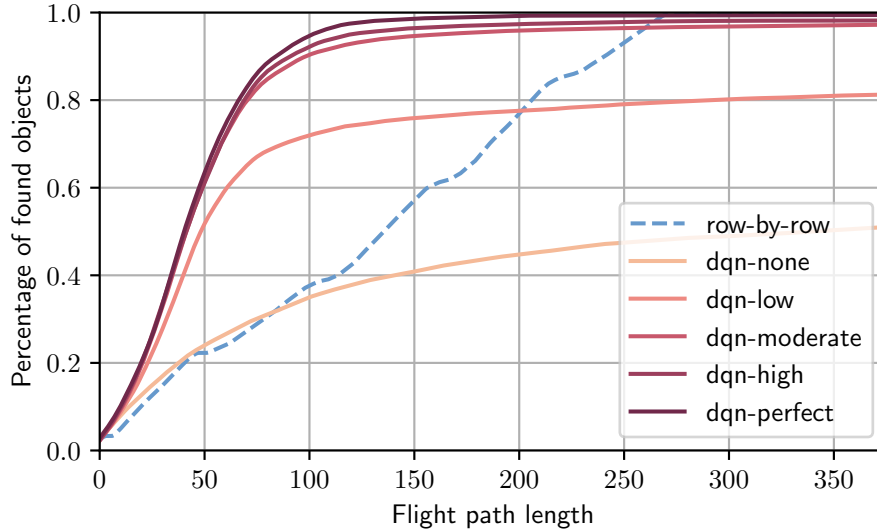


Figure 13: Effect of the different prior knowledge quality levels on the percentage of found objects for the policy learned by DQN, and the baseline row-by-row flight path. The lines show the mean over 1000 episodes.

Figure 14 shows some flight paths for the DQN agents with different levels of prior knowledge quality. Without prior knowledge (Figure 14a), the agent quickly found the objects around the start location of the drone based on information from the local map, but failed to find objects further away from the start location. When having perfect prior knowledge (Figure 14e), the agent quickly finds all objects without wandering around.

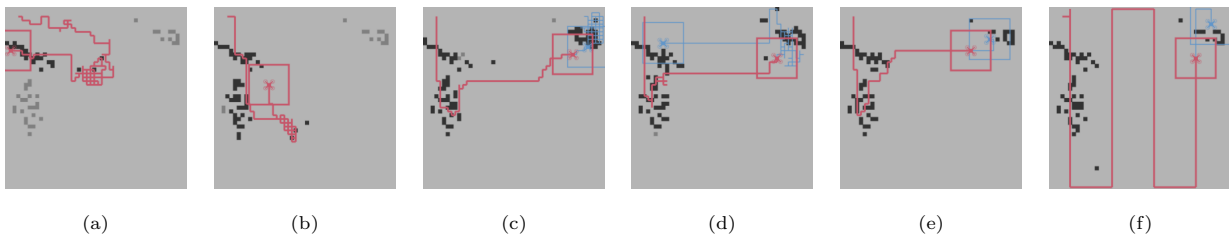


Figure 14: Single flight paths of the RL agent for prior knowledge quality level none (no prior knowledge) (a), low (b), moderate (c), high (d) and perfect (e) and the baseline row-by-row flight path (f). The detected objects are indicated with black dots and the not detected objects with gray dots. The red line indicates the flight path till 80% of the objects are found, the blue line the complete flight path till all objects were found or the battery was empty.

3.4. Experiment 4: Effect of different stopping criteria

Figure 15 shows the percentage of objects found and flight path length using different stopping criteria. Setting a threshold on coverage resulted in a high percentage of found objects, but also a long path length.

This indicates that the agent had difficulty fulfilling the coverage threshold before the battery was empty. Stopping the search task when there were no new detections during 15, 25 or 50 consecutive steps did result in a significantly shorter path length. However, terminating the task 15 or 25 steps after the last detection was too soon, indicated by the lower percentage of found objects. Terminating the search task when there were no new objects detected in the previous 50 steps resulted in a high number of found objects and a shorter flight path than the default stopping criterion (stop searching when all objects were found). Using a learned land action that terminates the search yielded a high percentage of found objects and a very short path length. When it is not essential to find all objects and a short flight path length is important, using a learned land action to terminate the search is suitable.

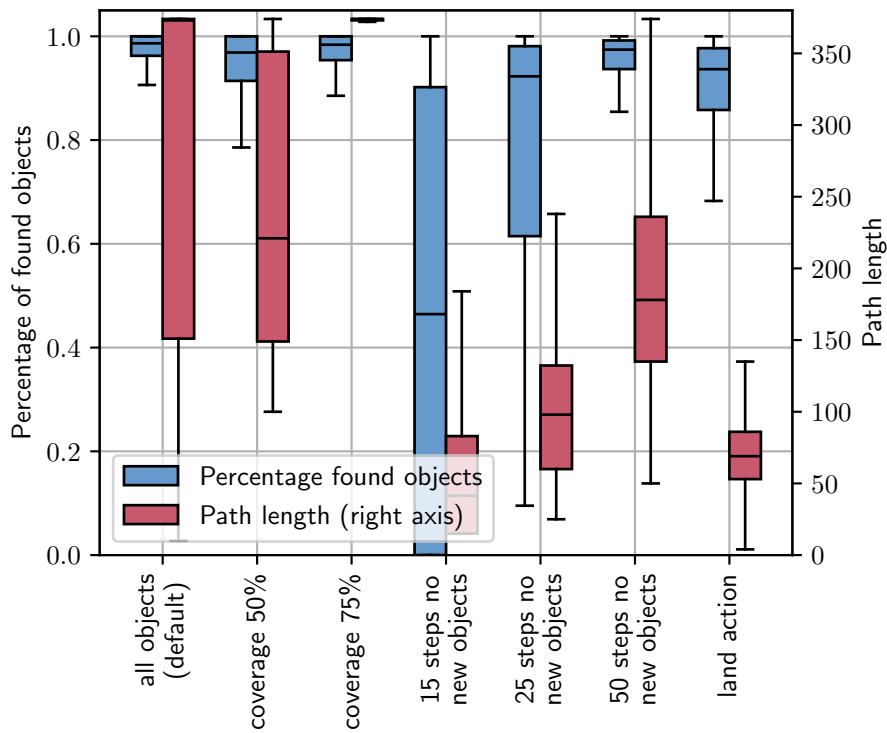


Figure 15: Boxplot showing the effect of different stopping criteria on the percentage of found objects and path length (right axis).

Figure 16 shows the distribution of the action value of the learned land action (after the softmax layer) compared to the percentage of found objects. As was expected, the number of times the land action got a high action value increased when the percentage of found objects increased, indicating that the agent learned that landing is only profitable after finding most objects. In 2% of the episodes, the drone landed directly without taking any flight actions.

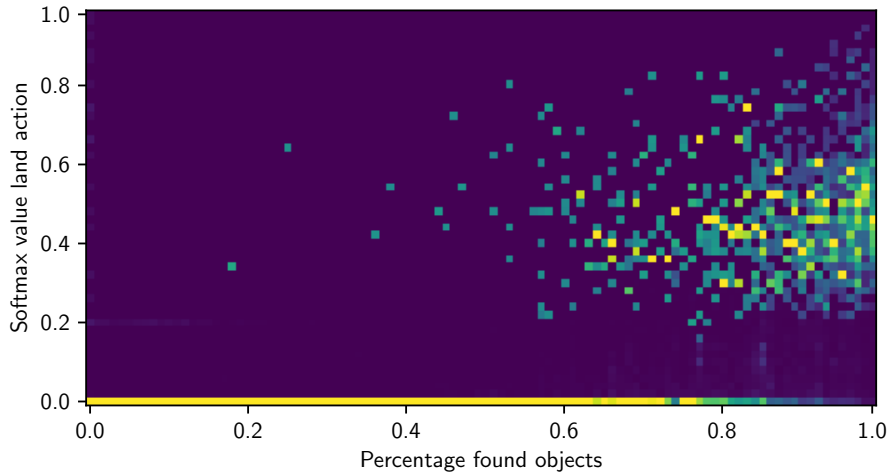


Figure 16: Histogram showing the relation between the action value after the softmax layer for the landing action and the percentage of found objects. The colors are normalized column-wise.

4. Discussion

The results showed that, with prior knowledge, the RL agent was able to find a shorter path than a baseline row-by-row flight path for finding the objects when they were non-uniformly distributed. Even with a low-quality prior knowledge and high number of detection errors, the learned search policy still outperformed a baseline row-by-row flight path in terms of path length and was able to find most objects. Especially when the objects are not uniformly distributed, there is great potential in a learned search policy over a traditional row-by-row flight path if a perfect mapping of objects is not required. When there was no perfect prior knowledge available, the RL agent still found most objects quicker than the row-by-row flight path, but was not able to find all objects. In section 4.1 we discuss the action selection by the agent, in section 4.2 the used action space, section 4.3 learning in absence of prior knowledge, section 4.4 the application and finally, section 4.5 discusses the influence of the assumptions on the applicability in the real world.

4.1. Action selection

Towards the end of some episodes, the agent sometimes got stuck in the same spot when not all objects were found by repeating the same two actions, such as 'fly north' and 'fly south' or 'fly east' and 'fly west' (Figure 14b for an example). Using a learned land action in experiment 4 solved this issue as it allowed the RL agent to decide when to terminate the search task and thus, when it was not profitable anymore to search for the last objects. However, we observed some cases where the drone directly terminated the

search task. This only happened in 2% of the episodes, in contrast to Yang et al. (2018) and Druon et al. (2020). Yang et al. (2018) indicated a 20-30% lower performance when using a stopping action and Druon et al. (2020) attributed around 50 percent of the failure cases to selecting the stopping action at the wrong moment. The difference in performance may be due to their use of an end-to-end network architecture that takes images as input, unlike the abstract representation used in this work. As these images have a larger variability than the abstract representation we use, the network is likely to be more uncertain about its predictions, which makes it more profitable to terminate earlier. To reduce the remaining 2% of direct terminations, a penalty for missing objects when landing could be introduced during training. This would encourage the agent to explore at least parts of the field before landing.

4.2. Action space

Similar to most research on RL-based path planning for UAVs (e.g. Guban and Haque (2023); Husnain et al. (2023)), in this work the environment is simplified into a 2D representation, where the UAV flies at a fixed altitude. To further increase the efficiency of the RL learned policy, the environment could be changed to 3D by involving actions for altitude changes, which can have several advantages for a search policy. In context of object search, it can be used to get a (low resolution) overview of the whole field at a high altitude, which can be used as prior knowledge in the global map. The drone can then learn to fly lower to inspect parts of the field in high resolution.

4.3. Learning in absence of prior knowledge

Experiment 3 showed that learning a search policy without any prior knowledge remained a challenge. Because the agent had no clue where the objects were, gathering useful state transition vectors for the experience replay buffer was difficult, which prevented the agent from learning useful actions. Possibly, curriculum learning can be used to gradually build up the challenge for the agent (Narvekar et al., 2020), starting with a simulation that has full prior knowledge and slowly building up to a simulation without prior knowledge.

4.4. Application

The usability of the presented learned policy depends on the type of application. When the goal of an application is to find most objects in a short period of time, the learned policy clearly outperforms the baseline row-by-row flight path. However, there is no guarantee that all objects are found, which limits the usability of such learned policy in applications where it is crucial to find all objects. For the use-case of

weed detection in arable fields, it may be fine to detect most weeds and miss some. Since weed detection requires multiple flights throughout the season, weeds that were not detected this flight can be detected in a later flight.

4.5. Impact of assumptions on applicability in the real world

Although the presented work was based on a abstracted simulated environment, the proposed method can easily be applied to a real-world scenario with a few additions. The simulator was designed to be used in combination with an object-detection system, prior knowledge information and a flight controller (Figure 1). With a trained detector, objects can be detected in a real camera image, which results in the object map input to the RL. The resulting discrete flight actions can be executed on a real drone using the drone’s flight controller. Below we discuss the underlying assumptions of the simulation and RL policy, as mentioned in the introduction and discuss the implications for real-world use:

Drone can accurately execute flight actions: the flight controller of the drone should be able to translate the discrete flight actions into motor signals. The discrete actions are in four directions with a distance determined by the grid-cell size. The localization accuracy of the drone should therefore be higher than the grid-cell size, to be able to accurately move the drone to a specific grid-cell. When using grid-cells of, for example, 1x1m, a drone equipped with RTK-GPS (accuracy of around 2-3cm) is more than accurate enough to execute the RL policy. As the use of RTK-GPS is quite standard on agricultural drones, this assumption can be met.

Field size: since the prior knowledge map is related to the field size and the Q-network uses a combination of convolutions and fully-connected layers (Figure 4), a larger field increases the size of the flattened layer and thereby the number of trainable parameters. This will require more training iterations. Experiment 3 showed that the number of found objects only dropped at a very low prior knowledge quality (and thus very low resolutions), which indicates that the resolution of the prior knowledge may be low. Therefore, larger fields can be used with the same number of trainable parameters by applying a larger down-sampling factor (increasing g_{global}), or by incorporating prior knowledge in a different way.

Prior knowledge of field boundaries: field boundaries are static and available on forehand. In this work, we limited the experiments to squared fields. Although not specifically tested, applying the learned search policy in non-squared fields can be achieved by changing the field-area map containing information if the cell is inside or outside the field. Additionally, obstacles within the field, such as trees, can be avoided by mapping them as non-field area. As the violation of the field-area map results in a negative reward, it is very likely that the RL agent will learn to deal with it. Work of Theile et al. (2021) showed that a

RL-learned policy with a comparable architecture is able to avoid buildings in a city when visiting specific locations using drones by encoding these positions in a no-fly-zone, which is in principle comparable with our field-area map.

A decently trained detection network: the results of experiment 2 showed that the RL agent is robust to errors in the object detection. Hence, the detection network does not have to be very accurate. Even when the detection network generates a lot of false positives, the RL policy was able to find most of the true positives. Typical object detection performance in agriculture lay around 0.7-0.9 F1-score (Rai et al., 2023; Ruigrok et al., 2023; Rehman et al., 2024). This roughly corresponds with level 'high' in experiment 2, which indicates that the RL agent can deal with input from a real field.

Prior knowledge of location of objects: although some level of prior knowledge is required, it does not need to be very detailed. Experiment 3 showed that the prior knowledge did not need to be very detailed or very accurate. This prior knowledge can be created by, for example, using the detections from a few higher altitude images, data from previous flights, or other data sources such as satellite images. For many agricultural tasks, like weed detection and disease detection, such rough prior knowledge is available. For instance, many weeds appear in the same area in subsequent years and spread very locally. Information from previous year can then be used as prior knowledge.

The above analysis indicates that all the underlying assumptions of the abstracted RL agent and simulation environment are not problematic for a real-world application of a RL learned search policy. Especially in use-cases where the target objects are distributed non-uniformly in the field and when it is not crucial to find all objects, there is much to gain when specifically searching for objects instead of flying over and covering the whole field.

5. Conclusion

In this study, we showed that a learned search policy can increase the efficiency of finding objects using a UAV, particularly when there was some prior knowledge available. When the objects were non-uniformly distributed, the learned search policy outperformed the baseline row-by-row flight path. The learned policy was robust against errors in the detection, and different qualities in prior knowledge only had minor influence on the number of found objects. In addition, the RL agent was able to learn when the search task had to be terminated and when it was not profitable to continue searching.

The major assumptions beneath the presented approach have limited impact on application in real-world

agricultural search tasks. For tasks that meet the assumptions as discussed in section 4.5, the method is expected to be applicable.

In conclusion, learning a search policy improves the efficiency of a search task for UAVs for applications where the target objects, such as weeds and disease infections, are non-uniformly distributed and when there is some level of prior knowledge. Learning to search objects in the absence of prior knowledge remains a topic for future work.

CRedit author statement

Rick van Essen: Conceptualization, Methodology, Formal analysis, Software, Visualization, Writing - Original Draft. **Eldert van Henten:** Conceptualization, Writing - Review & Editing, Funding acquisition. **Gert Kootstra:** Conceptualization, Methodology, Writing - Review & Editing, Funding acquisition.

Declaration of Competing Interest

This research is part of the research program SYNERGIA (project number 17626), which is partly financed by the Dutch Research Council (NWO).

Data availability

The simulation and RL network is made available on https://github.com/wur-abe/rl_drone_object_search.

References

- Albani, D., Manoni, T., Arik, A., Nardi, D., Trianni, V., 2019. Field Coverage for Weed Mapping: Toward Experiments with a UAV Swarm, in: Compagnoni, A., Casey, W., Cai, Y., Mishra, B. (Eds.), *Bio-inspired Information and Communication Technologies*, Springer International Publishing, Cham. pp. 132–146.
- Anul Haq, M., 2022. CNN Based Automated Weed Detection System Using UAV Imagery. *Computer Systems Science and Engineering* 42, 837–849. doi:10.32604/csse.2022.023016.
- Azar, A.T., Koubaa, A., Ali Mohamed, N., Ibrahim, H.A., Ibrahim, Z.F., Kazim, M., Ammar, A., Benjdira, B., Khamis, A.M., Hameed, I.A., Casalino, G., 2021. Drone Deep Reinforcement Learning: A Review. *Electronics* 10, 999. doi:10.3390/electronics10090999.
- Cardina, J., Johnson, G.A., Sparrow, D.H., 1997. The Nature and Consequence of Weed Spatial Distribution. *Weed Science* 45, 364–373. Publisher: [Cambridge University Press, Weed Science Society of America].
- Chin, R., Catal, C., Kassahun, A., 2023. Plant disease detection using drones in precision agriculture. *Precision Agriculture* 24, 1663–1682. doi:10.1007/s11119-023-10014-y.

- Druon, R., Yoshiyasu, Y., Kanezaki, A., Watt, A., 2020. Visual Object Search by Learning Spatial Context. *IEEE Robotics and Automation Letters* 5, 1279–1286. doi:10.1109/LRA.2020.2967677.
- Gao, J., Ye, W., Guo, J., Li, Z., 2020. Deep Reinforcement Learning for Indoor Mobile Robot Path Planning. *Sensors* 20, 5493. doi:10.3390/s20195493.
- Girshick, R., 2015. Fast R-CNN. ArXiv:1504.08083 [cs].
- Gugan, G., Haque, A., 2023. Path Planning for Autonomous Drones: Challenges and Future Directions. *Drones* 7, 169. doi:10.3390/drones7030169.
- Husnain, A., Mokhtar, N., Shah, N.M., Dahari, M., Iwahashi, M., 2023. A systematic literature review (slr) on autonomous path planning of unmanned aerial vehicles. *Drones* 2023, Vol. 7, Page 118 7, 118. doi:10.3390/DRONES7020118.
- Liu, C., Jian, Z., Xie, M., Cheng, I., 2021. A Real-Time Mobile Application for Cattle Tracking using Video Captured from a Drone, in: 2021 International Symposium on Networks, Computers and Communications (ISNCC), IEEE, Dubai, United Arab Emirates. doi:10.1109/isncc52172.2021.9615648.
- Lodel, M., Brito, B., Serra-Gomez, A., Ferranti, L., Babuska, R., Alonso-Mora, J., 2022. Where to Look Next: Learning Viewpoint Recommendations for Informative Trajectory Planning, in: 2022 International Conference on Robotics and Automation (ICRA), IEEE, Philadelphia, PA, USA. pp. 4466–4472. doi:10.1109/ICRA46639.2022.9812190.
- Mier, G., Valente, J., de Bruin, S., 2023. Fields2cover: An open-source coverage path planning library for unmanned agricultural vehicles. *IEEE Robotics and Automation Letters* 8, 2166–2172. doi:10.1109/LRA.2023.3248439.
- Mnih, V., Kavukcuoglu, K., Silver, D., Rusu, A.A., Veness, J., Bellemare, M.G., Graves, A., Riedmiller, M., Fidjeland, A.K., Ostroski, G., Petersen, S., Beattie, C., Sadik, A., Antonoglou, I., King, H., Kumaran, D., Wierstra, D., Legg, S., Hassabis, D., 2015. Human-level control through deep reinforcement learning. *Nature* 518, 529–533. doi:10.1038/nature14236.
- Narvekar, S., Peng, B., Leonetti, M., Sinapov, J., Taylor, M.E., Stone, P., 2020. Curriculum Learning for Reinforcement Learning Domains: A Framework and Survey. *J. Mach. Learn. Res.* 21. Publisher: JMLR.org.
- Niroui, F., Zhang, K., Kashino, Z., Nejat, G., 2019. Deep Reinforcement Learning Robot for Search and Rescue Applications: Exploration in Unknown Cluttered Environments. *IEEE Robotics and Automation Letters* 4, 610–617. doi:10.1109/LRA.2019.2891991.
- Panov, A.I., Yakovlev, K.S., Suvorov, R., 2018. Grid Path Planning with Deep Reinforcement Learning: Preliminary Results. *Procedia Computer Science* 123, 347–353. doi:10.1016/j.procs.2018.01.054.
- Pei, H., Sun, Y., Huang, H., Zhang, W., Sheng, J., Zhang, Z., 2022. Weed Detection in Maize Fields by UAV Images Based on Crop Row Preprocessing and Improved YOLOv4. *Agriculture* 12, 975. doi:10.3390/agriculture12070975.
- Raffin, A., Hill, A., Gleave, A., Kanervisto, A., Ernestus, M., Dormann, N., 2021. Stable-baselines3: Reliable reinforcement learning implementations. *Journal of Machine Learning Research* 22, 1–8.
- Rai, N., Zhang, Y., Ram, B.G., Schumacher, L., Yellavajjala, R.K., Bajwa, S., Sun, X., 2023. Applications of deep learning in precision weed management: A review. *Computers and Electronics in Agriculture* 206, 107698. doi:10.1016/j.compag.2023.107698.
- Rehman, M.U., Eesaar, H., Abbas, Z., Seneviratne, L., Hussain, I., Chong, K.T., 2024. Advanced drone-based weed detection using feature-enriched deep learning approach. *Knowledge-Based Systems* 305, 112655. doi:10.1016/j.knosys.2024.112655.
- Rejeb, A., Abdollahi, A., Rejeb, K., Treiblmaier, H., 2022. Drones in agriculture: A review and bibliometric analysis. *Computers and Electronics in Agriculture* 198, 107017. doi:10.1016/j.compag.2022.107017.
- Rivas, A., Chamoso, P., González-Briones, A., Corchado, J.M., 2018. Detection of Cattle Using Drones and Convolutional

- Neural Networks. *Sensors* 18, 2048. doi:10.3390/s18072048. publisher: MDPI AG.
- Ruigrok, T., Van Henten, E.J., Kootstra, G., 2023. Improved generalization of a plant-detection model for precision weed control. *Computers and Electronics in Agriculture* 204, 107554. doi:10.1016/j.compag.2022.107554.
- Sutton, R.S., Barto, A.G., 2018. Reinforcement learning: an introduction. MIT press, Cambridge, Massachusetts, USA.
- Theile, M., Bayerlein, H., Nai, R., Gesbert, D., Caccamo, M., 2020. UAV Coverage Path Planning under Varying Power Constraints using Deep Reinforcement Learning, in: 2020 IEEE/RSJ International Conference on Intelligent Robots and Systems (IROS), IEEE, Las Vegas, NV, USA. pp. 1444–1449. doi:10.1109/IROS45743.2020.9340934.
- Theile, M., Bayerlein, H., Nai, R., Gesbert, D., Caccamo, M., 2021. UAV Path Planning using Global and Local Map Information with Deep Reinforcement Learning, in: 2021 20th International Conference on Advanced Robotics (ICAR), IEEE, Ljubljana, Slovenia. pp. 539–546. doi:10.1109/ICAR53236.2021.9659413.
- Tu, G.T., Juang, J.G., 2023. Uav path planning and obstacle avoidance based on reinforcement learning in 3d environments. *Actuators* 2023, Vol. 12, Page 57 12, 57. doi:10.3390/ACT12020057.
- Xu, B., Fan, J., Chao, J., Arsenijevic, N., Werle, R., Zhang, Z., 2023a. Instance segmentation method for weed detection using UAV imagery in soybean fields. *Computers and Electronics in Agriculture* 211, 107994.
- Xu, K., Shu, L., Xie, Q., Song, M., Zhu, Y., Cao, W., Ni, J., 2023b. Precision weed detection in wheat fields for agriculture 4.0: A survey of enabling technologies, methods, and research challenges. *Computers and Electronics in Agriculture* 212, 108106. doi:10.1016/j.compag.2023.108106.
- Yang, W., Wang, X., Farhadi, A., Gupta, A., Mottaghi, R., 2018. Visual Semantic Navigation using Scene Priors. ArXiv:1810.06543 [cs].
- Yu, J., Su, Y., Liao, Y., 2020. The path planning of mobile robot by neural networks and hierarchical reinforcement learning. *Frontiers in Neurobotics* 14, 63. doi:10.3389/FNBOT.2020.00063/BIBTEX.
- Zhang, C., Valente, J., Wang, W., Guo, L., Tubau Comas, A., Van Dalflen, P., Rijk, B., Kooistra, L., 2023. Feasibility assessment of tree-level flower intensity quantification from UAV RGB imagery: A triennial study in an apple orchard. *ISPRS Journal of Photogrammetry and Remote Sensing* 197, 256–273. doi:10.1016/j.isprsjprs.2023.02.003. publisher: Elsevier BV.